ANGULAR POLARIZATION STRUCTURE OF LIGHT TRANSMITTED THROUGH A HOMEOTROPIC NEMATIC CELL

R.G. VOVK, A.D. KISELEV, I.A. BUINYI, M.S. SOSKIN

Institute of Physics, Nat. Acad. Sci. of Ukraine
(46, Nauka Ave., Kyiv 03680, Ukraine; e-mail: roman.vovk@gmail.com)

UDC 535.372

The polarization structure of light transmitted through a homeotropic cell filled with a nematic liquid crystal (NLC) has been found to be characterized by the availability of polarization singularities which arise owing to the interference of characteristic modes in the anisotropic substance. Stokes polarimetry has been used to measure the polarization-resolved conoscopic images. For a homeotropic cell, the parameters of polarization singularities in the angular distributions of polarization ellipses have been calculated analytically. The results of theoretical calculations agree well with experimental data.

1. Introduction

Optical properties of liquid crystals (LCs) are known to be very important for their numerous applications [1–3]. As a rule, LCs are used as an anisotropic medium, where the anisotropy is governed by its orientational structure, the latter being sensitive to external fields and to a change of boundary conditions.

Similarly as it is in other anisotropic materials, the polarization of light propagating in LC varies owing to the anisotropy of the latter. In an LC cell placed between crossed polarizers, these anisotropy-induced polarization changes reveal themselves in variations of the transmission coefficient. A significant number of experimental methods developed for studying the orientational structures in LC cells are based on this effect.

For instance, the known method of crystal rotation [4] involves the analysis of the angular dependence of LC-cell transmission in the configuration with crossed polarizers. Such a dependence can be considered as a one-dimensional cross-section of the more general (two-dimensional) conoscopic image.

Conoscopy is successfully used for studying the LC systems. In particular, it is applied to revealing the biaxiality of NLCs [5, 6] and measuring the pretilt angle [7, 8]. The conoscopic images of hybrid NLCs cells were also studied in work [9].

From the fundamental point of view, the problem of detailed study of the polarization structure, which conoscopic images originate from, naturally arises. In other words, the matter is about the analysis of the dependence of a light polarization state after the light transmission through LC cells on the angles of incidence. We will study the two-dimensional angular distributions of Stokes parameters, which describe the field of polarization ellipses; the latter can be referred to as a polarization-resolved conoscopic image.

Nye [10–12] was the first who demonstrated that the so-called polarization singularities are important elements which characterize the geometrical structure of polarization fields. In particular, these include C-points (the point of circular polarization) and L-curves (the curves of linear polarization).

In work [13], the theory of singularities has been applied to analyze the angular dependence of polarization (the polarization state of the electric induction vector) for the plane-wave characteristic modes of anisotropic crystals, including dichroic and chiral ones. In work [14], this analysis was extended – by applying the 4×4-matrix formalism – to include the case of bianisotropic crystals.

Experimental results and the results of calculations obtained in work [15] testify that, when a linearly polarized Laguerre–Gauss beam with a vortex on its axis propagates in an anisotropic crystal, there appears a complicated structure of polarization singularities.

In this work, we study the polarization structures that arise owing to the interference of four characteristic modes of a homeotropic NLC cell excited by a plane wave incident upon the cell. The method of Stokes polarimetry was used in order to measure the field of Stokes parameters which was presented in the form of a distribution of polarization ellipses. We also present the analytical results obtained for the characteristics of polarization singularities and compare the results of our calculations with experimental data.

2. Experimental Part

In our experiments, we used a homeotropic planar NLC cell 110 μm in thickness. The thickness spread was checked taking advantage of the interference technique and did not exceed ± 1 μm. The cell was filled with nematic E7 which is characterized by the ordinary refractive index $n_o \approx 1.5217$ and the extraordinary one $n_e \approx 1.7472$ in the optical range.

A coherent continuous single-frequency He-Ne laser with the wavelength $\lambda = 0.633$ μm and an emitting power of 10 mW was used as a radiation source. The experimental installation, whose scheme is presented in Fig. 1, was a modification of typical installations destined for studying the polarization distribution over the transverse cross-section of light beams [15, 16].

Light emitted by the He-Ne laser was collimated by lenses $L1$ and $L2$. Polarizer $P1$ was used to set the orientation for the polarization vector of the electric field of a linearly polarized wave. In experiments with circularly polarized light, polarizer $P1$ was followed by a quarter-wavelength plate.

Microobjective $L3$ was used to produce a divergent light beam. Microobjective $L4$ and lens $L5$ collimated the beam after its having transmitted through NLC cell NLC. Further, the beam was analyzed by a Stokes-analyzer (a quarter-wavelength plate and polarizer $P2$).

To determine the parameters of light polarization, we measured the intensities of four linearly polarized components with azimuths of 0, $\pi/4$, $\pi/2$, and $3\pi/4$: $I(0)$, $I(\pi/4)$, $I(\pi/2)$, and $I(3\pi/4)$, respectively; as well as the intensities of right- and left-circularly polarized components: I_+ and I_-, respectively. The values of the measured intensities were applied to calculate the Stokes

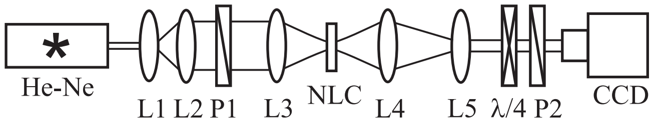

Fig. 1. Scheme of the experimental installation (see notations in the text)

parameters by formulas [17]

$$S_0 = I(0) + I(\pi/2) = \sqrt{S_1^2 + S_2^2 + S_3^2}, \tag{1a}$$

$$S_1 = I(0) - I(\pi/2) = S_0 \cos 2\chi_p \cos 2\phi_p, \tag{1b}$$

$$S_2 = I(\pi/4) - I(3\pi/4) = S_0 \cos 2\chi_p \sin 2\phi_p, \tag{1c}$$

$$S_3 = I_+ - I_- = S_0 \sin 2\chi_p, \tag{1d}$$

where the Poincaré sphere is parametrized in terms of the polarization azimuth ϕ_p ($0 < \phi_p \leq \pi$) and the ellipticity angle χ_p ($-\pi/4 \leq \chi_p \leq \pi/4$).

The geometrical characteristics of the polarization ellipse are the polarization azimuth ϕ_p, which sets the orientation of the long semi-axis of the ellipse in the plane that is perpendicular to the wave vector, and the ellipticity $\varepsilon_{\rm ell}$, whose amplitude is the ratio between the lengths of the short and long semi-axes of the ellipse. From Eqs. (1), one can see that those characteristics are coupled with the Stokes parameters in the following manner:

$$\phi_p = 2^{-1} \arg S, \quad S \equiv S_1 + iS_2, \tag{2}$$

$$\varepsilon_{\rm ell} = -\,\mathrm{tg}\,\chi_p, \quad \chi_p = 2^{-1} \arcsin(S_3/S_0). \tag{3}$$

In our installation, the required intensities of the field polarization components were fixed by a CCD-chamber. The data obtained were processed by a computer, and the Stokes parameters for every pixel were calculated by formulas (1).

The geometrical image of the distribution of Stokes parameters in the plane of a CCD-chamber is a two-dimensional field of polarization ellipses, with every ellipse being characterized by the polarization azimuth and the ellipticity which are calculated by formula (2) for every pixel. The results obtained are discussed in Section 4..

3. Polarization Singularities

3.1. Transmission matrix

Consider an NLC cell with thickness d, sandwiched between two substrates, the normals to which are

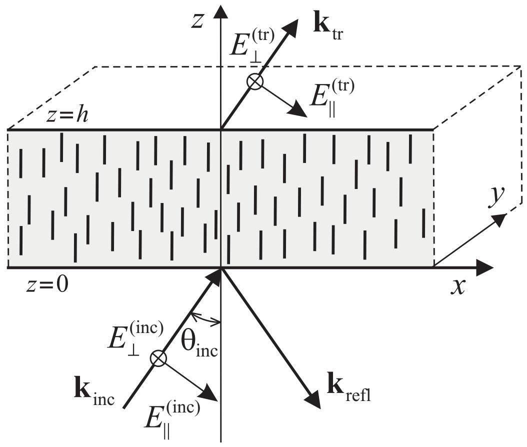

Fig. 2. Cross-section of the NLC cell in the plane of light incidence

directed along z axis: $z = 0$ and $z = d$. The general form of the dielectric tensor of NLC is [1]

$$\varepsilon = \varepsilon_\perp I_3 + \Delta\varepsilon\, \widehat{\mathbf{d}} \otimes \widehat{\mathbf{d}}, \tag{4}$$

where $\widehat{\mathbf{d}}$ is the NLC director, $\Delta\varepsilon = \varepsilon_\parallel - \varepsilon_\perp$, and I_3 is the unitary 3×3-matrix. For the overwhelming majority of known nematics, the anisotropy is uniaxial, and the eigenvalues of tensor (4) are equal to the ordinary and extraordinary refractive indices, $n_o = \sqrt{\mu\epsilon_\perp}$ and $n_e = \sqrt{\mu\epsilon_\parallel}$, respectively, where μ is the magnetic permeability of the NLC.

Let the external medium be isotropic, with the dielectric constant ϵ_m and the magnetic permeability μ_m. Figure 2 shows that there are two plane waves in the half-space $z \le 0$: an *incident* wave $\{\mathbf{E}_{\mathrm{inc}}, \mathbf{H}_{\mathrm{inc}}\}$ and a *reflected* one $\{\mathbf{E}_{\mathrm{refl}}, \mathbf{H}_{\mathrm{refl}}\}$. The *transmitted* wave $\{\mathbf{E}_{\mathrm{tr}}, \mathbf{H}_{\mathrm{tr}}\}$ and the reflected one are excited by the incident wave and propagate in the parallel direction in the half-space $z \ge d$. Therefore, the field outside the cell can be written down as

$$\mathbf{E}|_{z<0} = \mathbf{E}_{\mathrm{inc}}(\hat{\mathbf{k}}_{\mathrm{inc}})\mathrm{e}^{i(\mathbf{k}_{\mathrm{inc}}\cdot\mathbf{r})} + \mathbf{E}_{\mathrm{refl}}(\hat{\mathbf{k}}_{\mathrm{refl}})\mathrm{e}^{i(\mathbf{k}_{\mathrm{refl}}\cdot\mathbf{r})}, \tag{5a}$$

$$\mathbf{E}|_{z>d} = \mathbf{E}_{\mathrm{tr}}(\hat{\mathbf{k}}_{\mathrm{tr}})\mathrm{e}^{i(\mathbf{k}_{\mathrm{tr}}\cdot\mathbf{r})}, \tag{5b}$$

where the wave vectors $\mathbf{k}_{\mathrm{inc}}$, $\mathbf{k}_{\mathrm{refl}}$, and $\mathbf{k}_{\mathrm{tr}}$, owing to the boundary conditions

$$\boldsymbol{\mathcal{P}}(\hat{\mathbf{z}}) \cdot \left[\mathbf{E}|_{z=0+0} - \mathbf{E}|_{z=0-0}\right] = \tag{6a}$$
$$= \boldsymbol{\mathcal{P}}(\hat{\mathbf{z}}) \cdot \left[\mathbf{E}|_{z=d+0} - \mathbf{E}|_{z=d-0}\right] = 0,$$

$$\boldsymbol{\mathcal{P}}(\hat{\mathbf{z}}) \cdot \left[\mathbf{H}|_{z=0+0} - \mathbf{H}|_{z=0-0}\right] = \tag{6b}$$
$$= \boldsymbol{\mathcal{P}}(\hat{\mathbf{z}}) \cdot \left[\mathbf{H}|_{z=d+0} - \mathbf{H}|_{z=d-0}\right] = 0,$$

where $\boldsymbol{\mathcal{P}}(\hat{\mathbf{z}}) = \boldsymbol{\mathcal{I}}_3 - \hat{\mathbf{z}} \otimes \hat{\mathbf{z}}$ is the projector operator onto the cell plane ($x-y$ plane), lay in the plane of incidence.

Another consequence of the boundary conditions (6) is that the tangential components of the wave vectors are equal. Assuming that the incidence plane is the coordinate plane $x - z$, we obtain

$$\mathbf{k}_\alpha = k_{\mathrm{m}}\hat{\mathbf{k}}_\alpha = k_x\,\hat{\mathbf{x}} + k_z^{(\alpha)}\,\hat{\mathbf{z}}, \quad \alpha \in \{\mathrm{inc}, \mathrm{refl}, \mathrm{tr}\}, \tag{7}$$

where $k_{\mathrm{m}}/k_{\mathrm{vac}} = n_{\mathrm{m}} = \sqrt{\mu_{\mathrm{m}}\epsilon_{\mathrm{m}}}$ is the refractive index of the external medium, $k_{\mathrm{vac}} = \omega/c = 2\pi/\lambda$ is the wave number in vacuum, $k_x = k_{\mathrm{m}}\sin\theta_{\mathrm{inc}}$, and $k_z^{(\mathrm{inc})} = k_z^{(\mathrm{tr})} = -k_z^{(\mathrm{refl})} = k_{\mathrm{m}}\cos\theta_{\mathrm{inc}}$.

The vector amplitudes of the electric fields of plane waves are

$$\mathbf{E}_\alpha(\hat{\mathbf{k}}_\alpha) = E_\parallel^{(\alpha)}\mathbf{e}_x(\hat{\mathbf{k}}_\alpha) + E_\perp^{(\alpha)}\mathbf{e}_y(\hat{\mathbf{k}}_\alpha), \tag{8}$$

$$\mathbf{e}_x(\hat{\mathbf{k}}_\alpha) = k_{\mathrm{m}}^{-1}\big(k_z^{(\alpha)}\,\hat{\mathbf{x}} - k_x\,\hat{\mathbf{z}}\big), \quad \mathbf{e}_y(\hat{\mathbf{k}}_\alpha) = \hat{\mathbf{y}}. \tag{9}$$

The solution of the transmission problem has the form of a linear relation between the components of the incident and transmitted waves

$$\begin{pmatrix} E_\parallel^{(\mathrm{tr})} \\ E_\perp^{(\mathrm{tr})} \end{pmatrix} = \boldsymbol{\mathcal{T}} \begin{pmatrix} E_\parallel^{(\mathrm{inc})} \\ E_\perp^{(\mathrm{inc})} \end{pmatrix}, \tag{10}$$

where $\boldsymbol{\mathcal{T}}$ is the transmission matrix. The main difficulty consists in calculating this matrix.

Mathematical details, which are relevant to the exact solution of the transmission problem for uniform anisotropic media and the general theory of polarization-resolved images, can be found in work [18]. Below, we repeat in brief only the basic results obtained for a homeotropic NLC cell in the case where $\mathbf{d} = \hat{\mathbf{z}}$. In this case, the transmission matrix is diagonal, and the following expressions for its elements (transmission coefficients) can be derived [18]:

$$\boldsymbol{\mathcal{T}} = \mathrm{diag}(t_x, t_y), \quad t_{x,y} = 2\mu_{\mathrm{m}}\, n_{\mathrm{m}}^{-1}\cos\theta_{\mathrm{inc}}\tau_{x,y}^{-1}, \tag{11a}$$

$$\tau_x = 2\mu_{\mathrm{m}}\, n_{\mathrm{m}}^{-1}\cos\theta_{\mathrm{inc}}\cos\delta_e - i[q_z^{(e)}]^{-1}\sin\delta_e \times$$
$$\left[(\mu_{\mathrm{m}} n_o n_{\mathrm{m}}^{-1}\cos\theta_{\mathrm{inc}})^2 + (n_o^{-1}q_z^{(e)})^2\right], \tag{11b}$$

$$\tau_y = 2\mu_{\mathrm{m}}\, n_{\mathrm{m}}^{-1}\cos\theta_{\mathrm{inc}}\cos\delta_o - i[q_z^{(o)}]^{-1}\sin\delta_o \times$$
$$\left[\cos^2\theta_{\mathrm{inc}} + (\mu_{\mathrm{m}} n_{\mathrm{m}}^{-1} q_z^{(o)})^2\right], \tag{11c}$$

where

$$q_z^{(o)} = \sqrt{n_o^2 - n_m^2\sin^2\theta_{\mathrm{inc}}},$$

$$q_z^{(e)} = n_o n_e^{-1}\sqrt{n_e^2 - n_m^2\sin^2\theta_{\mathrm{inc}}}$$

and $\delta_\alpha = q_z^{(\alpha)} k_{\mathrm{vac}} d$.

3.2. C-points and L-curves

It is convenient to characterize the state of polarization in terms of the circular components of vector amplitudes

$$\mathbf{E}(\hat{\mathbf{k}}) = E_+\mathbf{e}_+(\hat{\mathbf{k}}) + E_-\mathbf{e}_-(\hat{\mathbf{k}}), \tag{12a}$$

$$E_\pm = 2^{-1/2}\big(E_\parallel \mp iE_\perp\big) = \big|E_\pm\big|\exp\{i\phi_\pm\}, \tag{12b}$$

where $\sqrt{2}\mathbf{e}_\pm(\hat{\mathbf{k}}) = \mathbf{e}_x(\hat{\mathbf{k}}) \pm i\mathbf{e}_y(\hat{\mathbf{k}})$. The main axes of the polarization ellipse are directed along the unit vectors $\mathbf{e}'_x(\hat{\mathbf{k}}) = \cos\phi_p\ \mathbf{e}_x(\hat{\mathbf{k}}) + \sin\phi_p\ \mathbf{e}_y(\hat{\mathbf{k}})$ and $\mathbf{e}'_y(\hat{\mathbf{k}}) = -\sin\phi_p\ \mathbf{e}_x(\hat{\mathbf{k}}) + \cos\phi_p\ \mathbf{e}_y(\hat{\mathbf{k}})$.

The polarization azimuth (2) and the ellipticity parameter (3), whose signs are different for the right and left polarizations, are determined by the formulas

$$\phi_p = (\phi_- - \phi_+)/2, \quad \varepsilon_{\mathrm{ell}} = \frac{|E_-| - |E_+|}{|E_-| + |E_+|}. \tag{13}$$

For the Stokes parameters (1), we have

$$S_1 = 2\mathrm{Re}E_+^* E_-, \quad S_2 = 2\mathrm{Im}E_+^* E_-, \tag{14a}$$

$$S_3 = |E_+|^2 - |E_-|^2, \quad S_0 = |E_+|^2 + |E_-|^2. \tag{14b}$$

If $|E_\nu| = 0$, the wave is circularly polarized, and the phases ϕ_ν and ϕ_p are indefinite. Therefore, such a polarization singularity can be regarded as a phase singularity of the complex Stokes field $S = S_1 + iS_2$. The points, where $|E_\nu| = 0$ and $\varepsilon_{\mathrm{ell}} = \nu$, will be referred to as C_ν-points.

In the case of linear polarization, the equality $|E_+| = |E_-|$ is valid, and the sign of polarization is indefinite. The curves of linear polarization are called L-curves.

The transmission matrix

$$\tilde{\boldsymbol{\mathcal{T}}}(\rho,\phi) = \exp(-i\phi\,\boldsymbol{\sigma}_3)\boldsymbol{\mathcal{T}}_c(\rho)\exp(i\phi\,\boldsymbol{\sigma}_3), \tag{15}$$

$$\rho = r\,\mathrm{tg}\,\theta_{\mathrm{inc}}, \quad \phi = \phi_{\mathrm{inc}}, \tag{16}$$

where $\boldsymbol{\mathcal{T}}_c = \boldsymbol{\mathcal{C}}\boldsymbol{\mathcal{T}}\boldsymbol{\mathcal{C}}^\dagger$, $\boldsymbol{\mathcal{C}} = 2^{-1/2}\begin{pmatrix}1 & -i\\ 1 & i\end{pmatrix}$, and $\boldsymbol{\sigma}_3 = \mathrm{diag}(1,-1)$, describes a conoscopic image on the plane, for which ρ and ϕ are the polar coordinates (the corresponding Cartesian coordinates are $x = \rho\cos\phi$ and $y = \rho\sin\phi$), and r is the scale factor dependent on the aperture.

Let the incident wave be linearly polarized along the vector $\cos\psi_p\ \mathbf{e}_x(\hat{\mathbf{k}}_{\mathrm{inc}}) + \sin\psi_p\ \mathbf{e}_y(\hat{\mathbf{k}}_{\mathrm{inc}})$. In this case, $E_\nu^{(\mathrm{inc})} = \exp(-\nu\psi_p)|E_{\mathrm{inc}}|$, and, for the transmitted wave, we have

$$\Psi_\nu = \big[(t_x + t_y) + (t_x - t_y)\exp(-2i\nu\psi)\big]\exp(-i\nu\psi_p), \tag{17}$$

where $\Psi_\nu = 2E_\nu^{(\mathrm{tr})}/|E_{\mathrm{inc}}|$ and $\psi = \phi - \psi_p$.

The C-points are located on circles, whose radii are found from the equation

$$R(\rho)\mathrm{Re}(t_x t_y^*) = |t_x|\cdot|t_y|\cos\delta = 0. \tag{18}$$

For weakly anisotropic NLCs, the δ-phase difference slightly differs from the phase taper $\delta \approx \delta_e - \delta_o$. From Eq. (18), it is evident that $\delta = \pi/2 + \pi k$, where the number $k = 0, 1, \ldots, N-1$ enumerates circles, ranging their radii ρ_k in ascending order.

From the expression for the amplitude

$$|\Psi_\nu(\rho_k,\phi)|^2 = 2\,|t|^2\big[1 + \cos 2\{\psi - \nu(-1)^k\alpha\}\big], \tag{19}$$

$$|t|^2 = |t_x|^2 + |t_y|^2, \quad \tan\alpha = \frac{|t_y|}{|t_x|}, \tag{20}$$

it becomes clear that every circle contains two pairs of C-points with the azimuthal angles

$$\phi_{\pm k}^{(\nu)} = \psi_p \pm \pi/2 + \nu(-1)^k\alpha. \tag{21}$$

It can be demonstrated that the C-point index, which is twice lower than the topological index of the complex field S [19], is calculated by the formula

$$I_C = \frac{\nu}{2}\,\mathrm{sign}\Big[\mathrm{Im}(\partial_x\Psi_\nu\,\partial_y\Psi_\nu^*)\Big]_{\substack{x=x_\nu\\ y=y_\nu}} = \tag{22}$$

$$= \frac{\nu}{2}\,\mathrm{sign}\Big[\mathrm{Im}(\partial_\rho\Psi_\nu\,\partial_\phi\Psi_\nu^*)\Big]_{\substack{\rho=\rho_\nu\\ \phi=\phi_\nu}}.$$

Accordingly, the following result is obtained:

$$I_C = -\frac{1}{2}\,\partial_\rho R(\rho)\Big|_{\rho=\rho_k} = \frac{(-1)^k}{2}. \tag{23}$$

The effect of the alternation for the polarization and C-point index signs is illustrated in Fig. 3 (panels b and d, respectively).

We can derive an analytical expression for the discriminant D_L, the sign of which determines the type of a C-point according to the classification by the number of straight rays N_C crossing the singularity [20]. The discriminant looks like

$$D_L = (R_1/|t|^2 + 1)^2 + \alpha_1^2 - 1, \tag{24}$$

$$R_1 \equiv (\rho\partial_\rho R)\Big|_{\rho=\rho_k}, \quad \alpha_1 \equiv (\rho\partial_\rho\alpha)\Big|_{\rho=\rho_k}. \tag{25}$$

If $D_L > 0$, then $N_C = 3$, and the C-point will be of the *star* or *monstar* type, depending on $I_C = -1/2$ or $I_C = +1/2$, respectively. It is easy to see that, at $I_C = -1/2$, the derivative R_1 is positive, so that such

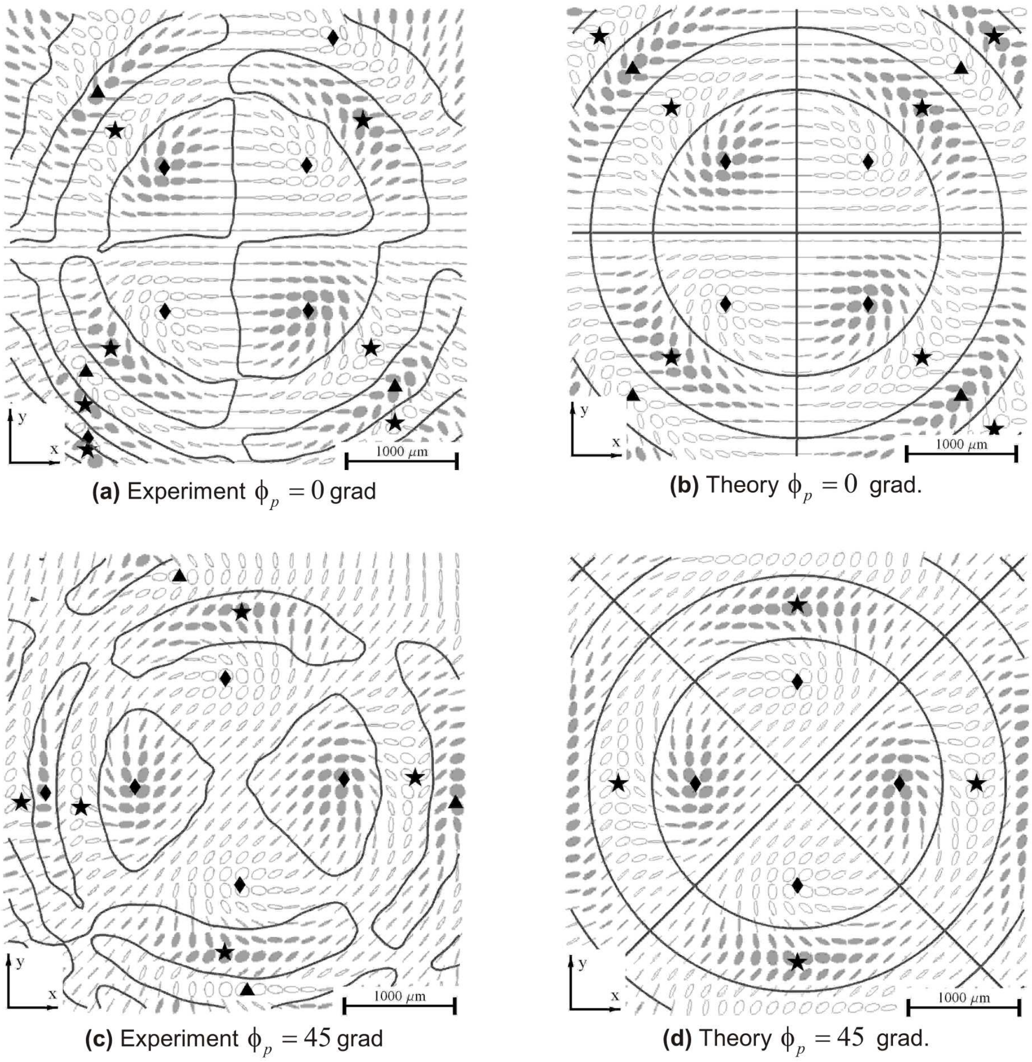

Fig. 3. Angular polarization patterns are shown as the fields of polarization ellipses in the plane with coordinates $x = \rho\cos\phi$ and $y = \rho\sin\phi$. The lemons and monstars are depicted as rhombs and triangles, respectively. Curves correspond to L-curves. Incident light is polarized linearly. Grayed ellipses correspond to the right polarization of light

points are always of the star type. The monstar type arises if the amplitudes of the transmission coefficient gradients are large enough. For example, let $R_1 < -2|t|^2$. In cells that are thick enough, all C-points with $k > 1$ and $I_C = +1/2$ will be monstars. If $k = 0$ (the conditions are close to normal incidence), then $D_L < 0$, and C-points are always of the *lemon* type, which is characterized by the equalities $N_C = 1$ and $I_C = +1/2$.

The equation

$$\mathrm{Im}(t_x t_y^*)\sin 2\psi = 0 \tag{26}$$

describes L-curves. There are evidently two straight lines $\phi = \psi_p$ and $\phi = \psi_p + \pi/2$, where the polarization vectors of the incident and transmitted waves are parallel to each other: $\phi_p = \psi_p$. The other L-curves are circles, the radii of which are the solutions of the equation $\delta = \pi k$ with $k = 1, \ldots, N-1$. It can be demonstrated that $\phi_p \approx \psi_p$ for even k's and $\phi_p \approx \psi_p + 2\phi$ for odd ones. It is also evident from Fig. 3 (panels a and c).

4. Comparison of the Theory with Experiment

While making theoretical calculations, the value of aperture-dependent scale factor (see Eq. (16)), which determines the radii of circles containing C-points, was taken to be 7 mm. This factor depends on the angle of the beam divergence aperture: the smaller the divergence angle of the beam, the smaller are the radii of the circles, on which the C-points are located. If the value of the quantity $r \tan\theta_{\rm inc}$ (see Eq. (16)) is less than that of ρ_0 (see Eq. (18)), the C-points cannot be resolved experimentally; it is the case close to normal incidence.

In Fig. 3, the angular polarization structures, both experimentally measured (panels *a* and *c*) and theoretically calculated (panels *b* and *d*), are depicted. The presented patterns illustrate the alternation effect for the topological sign of C-points, which is described by Eq. (23). In full accordance with the theory (Eq. (23)), at the center of the polarization-resolved conoscopic image (Fig. 3) there are four C-points of the lemon type. On the next circle, where the gradient amplitudes for the transmission coefficients start to increase, there appear C-points of the star – according to Eq. (18) – and monstar – according to Eq. (24) – types. It should be noted that the polarization structure does not change as the polarization azimuth of incident light varies, but only rotates by the angle equal to the azimuthal one (see Eq. (21)).

The L-curves in the theoretically calculated angular polarization patterns (Figs. 3,*b* and 3,*d*) form two coordinate axes, which rotate together with the azimuth, and concentric L-circles, which separate circles containing C-points. In the experimentally obtained patterns, the L-curves do not form a continuous grid of straight lines and circles. Instead, the grid of L-curves decays into a set of closed contours (Figs. 3,*a* and 3,*c*), which is explained by the inhomogeneity of the LC cells, as well as by the influence of the light scattering by director's fluctuations, which gives rise to a change of the light polarization state after light having been transmitted through the LC cell.

5. Conclusions

The angular distributions of polarization ellipses, which reflect the polarization structures – the origin of conoscopic images, – have been obtained. On the basis of the exact solution derived for the transmission problem, the characteristics of the polarization singularities in those distributions have been analyzed theoretically. In particular, C-points were demonstrated to form symmetrically located radial structures, and the topological index of C-points was shown to alternate its sign while crossing the boundaries of those structures. The comparison of theoretical results with experimental data evidences for good agreement between them.

1. P.G. de Gennes and J. Prost, *The Physics of Liquid Crystals* (Oxford, Clarendon Press, 1993).
2. P. Yeh and C. Gu, *Optics of Liquid Crystal Displays* (Wiley, Singapore, 1999).
3. V.G. Chigrinov, *Liquid Crystal Devices: Physics and Applications* (Boston, Artech House, 1999).
4. G. Baur, V. Wittwer, and D.W. Berreman, Phys. Lett. A **56**, 142 (1976).
5. L.J. Yu and A. Saupe, Phys. Rev. Lett. **45**, 1000 (1980).
6. L.A. Madsen, T.J. Dingemans, M. Nakata, and E.T. Samulski, Phys.Rev. Lett. **92**, 145505 (2004).
7. L. Komitov, G. Hauk, and H.D. Koswig, Cryst. Res. Technol. **19**, 253 (1984).
8. L.H. Brett and H.H. Winter, Appl. Opt. **40**, 2089 (2001).
9. Yu.A. Nastishin, O.B. Dovgyi, and O.G. Vlokh, Ukr. J. Phys. Opt. **2**, 98 (2001).
10. J.F. Nye, Proc. R. Soc. Lond. A **389**, 279 (1983).
11. J.F. Nye and J.V. Hajnal, Proc. R. Soc. Lond. A **409**, 21 (1987).
12. J.F. Nye, *Natural Focusing and Fine Structure of Light: Caustics and Wave Dislocations* (Institute of Physics Publishing, Bristol, 1999).
13. M.V. Berry and M.R. Dennis, Proc. R. Soc. Lond. A **459**, 1261 (2003).
14. M.V. Berry, Proc. R. Soc. Lond. A **461**, 2071 (2005).
15. F. Flossmann, U.T. Schwarz, and M.R. Dennis, Phys. Rev. Lett. **95**, 253901 (2005).
16. M.S. Soskin, V. Denisenko, and I. Freund, Opt. Lett. **28**, 1475 (2003).
17. M. Born and E. Wolf, *Principles of Optics*, 2nd ed. (Pergamon Press, Oxford, UK, 1980).
18. A.D. Kiselev, physics/0612114 (unpublished).
19. N.D. Mermin, Rev. Mod. Phys. **51**, 591 (1979).
20. M.V. Berry and J.H. Hannay, J. Phys. A.: Math. Gen. **10**, 1809 (1977).

Received 15.01.07.
Translated from Ukrainian by O.I.Voitenko

КУТОВА ПОЛЯРИЗАЦІЙНА СТРУКТУРА
ПРОПУСКАННЯ ГОМЕОТРОПНОЇ
КОМІРКИ НЕМАТИКА

Р.Г. Вовк, О.Д. Кисельов, І.О. Буйний, М.С. Соскін

Р е з ю м е

Знайдено, що поляризаційна структура світла після проходження гомеотропно орієнтованої комірки, заповненої нематичним рідким кристалом (НРК), характеризується наявністю поляризаційних сингулярностей, які виникають внаслідок інтерференції власних хвиль анізотропного середовища. Вимірювання поляризаційно розділених коноскопічних зображень було виконано за допомогою методу стокс-поляриметрії. Для гомеотропної комірки характеристики поляризаційних сингулярностей в кутових розподілах еліпсів поляризації обчислено аналітично. Показано, що результати теоретичних розрахунків добре узгоджуються з експериментальними даними.